J Geod
DOI 10.1007/s00190-010-0393-3

ORIGINAL ARTICLE

On the importance of accurately ray-traced troposphere corrections for Interferometric SAR data

Thomas Hobiger · Youhei Kinoshita · Shingo Shimizu · Ryuichi Ichikawa · Masato Furuya · Tetsuro Kondo · Yasuhiro Koyama

Received: 9 October 2009 / Accepted: 27 May 2010

Abstract Numerical weather models offer the possibility to compute corrections for a variety of space geodetic applications, including remote sensing techniques like interferometric SAR. Due to the computational complexity, exact ray-tracing is avoided in many cases and mapping approaches are applied to transform vertically integrated delay corrections into slant direction. Such an approach works well as long as lateral atmospheric gradients are small enough to be neglected. But since such an approximation holds only for very rare cases it is investigated how horizontal gradients of different atmospheric constituents can evoke errors caused by the mapping strategy. Moreover, it is discussed how sudden changes of wet refractivity can easily lead to millimeter order biases when simplified methods are applied instead of ray-tracing. By an example, based on real InSAR data, the differences of the various troposphere correction schemes are evaluated and it is shown how the interpretation of the geophysical signals can be affected. In addition, it is studied to which extend troposphere noise can be reduced by applying the exact ray-tracing solution.

Keywords InSAR · Troposphere delay · Ray-tracing · Numerical weather model

T. Hobiger (✉) · Y. Koyama
Space-Time Standards Group,
National Institute of Information and Communications Technology (NICT), 4-2-1 Nukui-Kitamachi, Koganei, Tokyo 184-8795, Japan
e-mail: hobiger@nict.go.jp

Y. Koyama
e-mail: koyama@nict.go.jp

Y. Kinoshita · M. Furuya
Department of Natural History Sciences, Hokkaido University, N10 W8, Kita-ku, Sapporo 060-0810, Japan
e-mail: youhei_skt@mail.sci.hokudai.ac.jp

M. Furuya
e-mail: furuya@mail.sci.hokudai.ac.jp

S. Shimizu
National Research Institute for Earth Science and Disaster Prevention, 3-1 Tennodai, Tsukuba, Ibaraki 305-0006, Japan
e-mail: shimizus@bosai.go.jp

R. Ichikawa · T. Kondo
Space-Time Standards Group, Kashima Space Research Center, National Institute of Information and Communications Technology (NICT), 893-1 Hirai, Kashima, Ibaraki 314-0012, Japan
e-mail: richi@nict.go.jp

T. Kondo
e-mail: kondo@nict.go.jp

1 Introduction

Interferometric synthetic aperture radar (InSAR) suffers, like any other space geodetic technique, from the fact that radio waves are delayed and bent when they propagate through the Earth's atmosphere, an effect known as troposphere refraction (e.g., Hanssen 2001). Although InSAR images are differential measurements the weather conditions between the satellite passages are changing and thus a signature of the atmosphere will bias the image. Such artifacts are mainly caused by two factors. The first, evoked by the water vapor content of the atmosphere, subsumed in the following as "wet delay", is difficult to be removed from a single InSAR image without any external information. Although this fraction accounts for only up to 10% of the total troposphere delay, the water vapor fields, with their highly spatial and temporal variations, make it difficult to predict or model this error source. Exploiting these characteristics, however, one can virtually eliminate the wet delay signals by stacking many independent InSAR images so that we can derive small secular deformation signals (e.g., Furuya et al. 2007).

Published online: 11 June 2010

On the other hand, the second part, i.e., the hydrostatic (also called "dry") delay component has a more predictable behavior, showing variations with much longer wavelengths. Moreover, the fact that the hydrostatic component decreases exponentially with height allows to remove a large fraction of this error source within the post-processing process together with the so-called topographic correction (Fujiwara et al. 1999). Nevertheless, such a simplified corrective scheme is not capable to represent hydrostatic delay effects completely. Thus, given the accurate information about the spatial and temporal distribution of atmospheric constituents [as e.g., provided by numerical weather models (NWM)], the most straightforward way to eliminate troposphere delays from InSAR images is provided by means of total delay.

2 Ray-tracing considerations

Earlier studies which dealt with troposphere delays based on numerical weather models (Wadge et al. 2002; Foster et al. 2006) avoided the complex computation of ray-traced delays and used vertically integrated values of atmospheric delay instead. Such values were mapped into slant direction using the first-order approximation that delays grow proportional to $\frac{1}{\cos i}$, where i denotes the incident angle of the scanning rays. If this "mapping approach" is strictly applied, one has to compute this angle for each pixel of an InSAR image, considering that the local incident angle is not constant throughout the image. Although a low orbit height of the satellite and a rather large extent of the scanned area on the ground can lead to a variation of the incident angles of several degrees, some studies even avoided the computation of exact geometric relations and applied an average incident angle, valid throughout the image. Besides errors introduced from such simplifications one has to take into consideration that the "mapping approach" assumes that lateral gradients of atmospheric conditions are small enough to justify the simple mathematical relation between zenith delays and those mapped into direction of the satellite.

2.1 Computation of ray-traced troposphere delays: solution of the boundary value problem

Other than mapping the delays with the corresponding incident angle factor one can also compute the exact ray-path through the numerical weather model and integrate the troposphere delay along this trajectory. This approach requires much more computational efforts than the strategies mentioned before, but allows to treat the whole problem in a consistent and straightforward way, which is only depending on the accuracy of the numerical weather model. Thus, given that such models are available for the area which has been targeted by InSAR, one can compute the 3D refractivity field from fundamental atmosphere quantities as described by Smith and Weintraub (1953) or boudouris (1963). Based on this information it is possible to compute the ray-path, by solving the Eikonal equation (Paris and Hurd 1969)

$$\sum_{i=1}^{3}\left(\frac{\partial\varphi(\mathbf{r})}{\partial r_i}\right)^2 = n^2(\mathbf{r}), \tag{1}$$

where $n(\mathbf{r})$ is the index of refractivity at position $\mathbf{r}$ and the expression $\varphi(\mathbf{r})$ is referred to as the Eikonal. In a ray-based coordinate system, Eq. 1 reads as

$$\frac{\mathrm{d}}{\mathrm{d}s}\left(n(\mathbf{r})\frac{\mathbf{dr}}{\mathrm{d}s}\right) = \nabla n(\mathbf{r}). \tag{2}$$

This equation can be split into two coupled first-order differential equations and solved by standard methods. Once the trajectory has been found, the troposphere delay $\Delta\tau_a$, can be computed as follows.

$$\Delta\tau_a = \underbrace{\int_{\text{atm}} (n(\mathbf{r})-1)\,\mathrm{d}s}_{\Delta\tau_e} + \underbrace{\int_{\text{atm}} \mathrm{d}s - \int_{\text{vac}} \mathrm{d}s}_{\Delta\tau_g}. \tag{3}$$

The first integral in Eq. 3 is evaluated along the path of the ray from the transmitter, through the atmosphere, until it reaches the ground-point and yields the electromagnetic delay $\Delta\tau_e$. The second term denotes the geometric excess resulting from the variation in the path of the ray as it passes through the atmosphere as compared to its path when propagating through vacuum. If scattering effects at the ground can be neglected and perfect reflection can be assumed, the incoming and reflected rays will coincide in their trajectories and only one half of the ray-path needs to be computed. Although the Eikonal problem can be approximated with sufficient accuracy by much faster algorithms (see Hobiger et al. 2008), we will solve the equation for each ray in order to be utmost consistent with the underlying physics and take the fine-scale information of the numerical weather models properly into account.

2.2 Computational aspects

Reciprocity of the Eikonal problem allows us to compute either the trajectory starting from the satellite to the ground or the other way, yielding identical results. Since a dedicated software package for the computation of ray-traced delays has been already designed for other space geodetic techniques (Hobiger et al. 2008) advantage of that previous work has been taken by computing all ray-traced corrections starting from the ground points. Nevertheless, due to the relatively low orbit height of remote sensing satellites, compared to GNSS beacons, it was necessary to revise some model components before they can be used for InSAR applications.

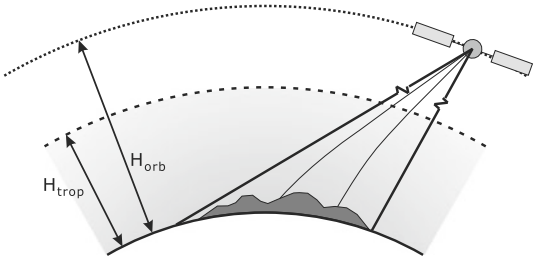

Fig. 1 Sketch of the geometric situation of SAR. Rays are delayed and bent by the atmosphere. Since the index of refractivity above $H_{\text{trop}} = 86\,\text{km}$ is very close to one, a straight line propagation without any additional delay can be assumed. H_{orb} reflects the height of the satellite with respect to the ground and is usually in the range of a few 100 km for remote sensing missions

Figure 1 outlines the overall situation for such a ray-tracing task. Since numerical weather information data are only available up to a certain height, which in our case is equal to $H_{\text{trop}} = 86\,\text{km}$, assumptions about the ray-propagation outside that region need to be made. Refractivity values are very close to zero for heights above 86 km, which makes it possible to assume that no electromagnetic and geometric delay contributions add to the total troposphere delay. Therefore, it is possible to carry out ray-tracing until the uppermost model height has been reached and assume a vacuum-like ray-propagation for the rest of the path. Radio sources of space geodetic techniques like GPS or very long baseline interferometry (VLBI) appear to be located far enough to solve the Eikonal equation in form of an initial value problem, based on the observing geometry (i.e., azimuth and elevation angles) of vacuum propagation. But since SAR satellites are orbiting at most 500–700 km above the Earth's surface, such an approach might not be appropriate for the solution of the ray-tracing problem. Thus, for utmost accurate results, it is mandatory to solve the boundary value problem, defined by the location of the transmitter (satellite) and receiver (ground point), based on the 3D refractivity field. A solution for this problem can be found by varying the ray-vector at the initial (ground) point until the target (i.e., the transmitter location) is hit within a certain threshold. Thus, the boundary value problem can be replaced by an initial value problem by varying the ground geometry in a self-correcting loop until the threshold criteria are fulfilled. For our studies we set the threshold to 0.1 m, i.e., we stopped after the ray was within a distance of 0.1 m, from the computed satellite position. This allows to carry out the computations with the algorithms described in detail in Hobiger et al. (2008) which will be very time-consuming, especially under consideration that a huge number of pixels will be processed for each SAR image. Solutions, taking advantage of parallel processing techniques, as discussed in Hobiger et al. (2009), allow to compute ray-traced troposphere corrections in significantly less time yielding identical results as those obtained from classical approaches.

3 Ray-tracing versus mapping approach

In order to evaluate whether the complex ray-tracing solution is required for the correction of remote sensing observations or if the mapping approach is sufficiently accurate, we start a simple scenario based on an arbitrary vertical troposphere profile. We do not intend to deduce a general relationship for errors introduced by the mapping approach, but just try to study effects from a single profile to get an idea whether we should use ray-tracing for the correction of InSAR data. Figure 2 depicts temperature, pressure, and relative humidity profiles extracted from the meso-scale analysis model (MANAL) from the Japanese Meteorologic Agency (JMA) for a grid point located close to Sapporo, Japan on 1 January 2008, 0 h UT. Pressure and temperature were extrapolated to 86 km height using the US Standard Atmosphere model as described in World Meteorological Organization (2000). Thereafter, refractivity along the profile can be computed according to the formalism described in Hobiger et al. (2008). This work serves also as reference for the solution of the ray-tracing problem, based on the Eikonal model and a spherical Earth. Thus, computing total troposphere delays for different zenith distances (or incident angles in the case of SAR) allows us to draw conclusions how well the simple mapping approach works.

3.1 Lateral gradients and small-scale structures

Instead of an isotropic atmosphere, anisotropy can be simulated by introducing lateral (i.e., horizontal) gradients of the three constituents, namely, temperature, pressure, and relative humidity. Thereby the effect of relative changes over a spherical distance of one degree is evaluated, e.g., a gradient of 1%/degree means that the value of the constituent changes by 1% in a distance of about 1° (111 km), is affected by a change of 0.5% at 55 km distance (0.5°), and so on. This scheme can be applied to pressure and relative humidity as shown in Fig. 2. To consider a realistic temperature variation, the effect of the gradient is also scaled with height, having 100% impact at zero height and decreasing linearly until reaching the upper height at 86 km. Based on empirical values deduced from numerical weather models, we allow temperature to vary by a maximum of ±2.5%, relative humidity by ±50% and pressure by ±0.25% over a spherical distance of 1°. These numbers represent the range of feasible changes at a given day, but may be slightly smaller or larger for different seasons and weather situations. If we vary one of the three constituents according to these numbers and keep the other two constant we can evaluate how much the mapping approach differs from the exact ray-tracing solution. Figure 3 shows the results from such a study. One can see that an error of at least 1 mm is introduced for incident angles over 25° when the mapping approach is used instead of exact

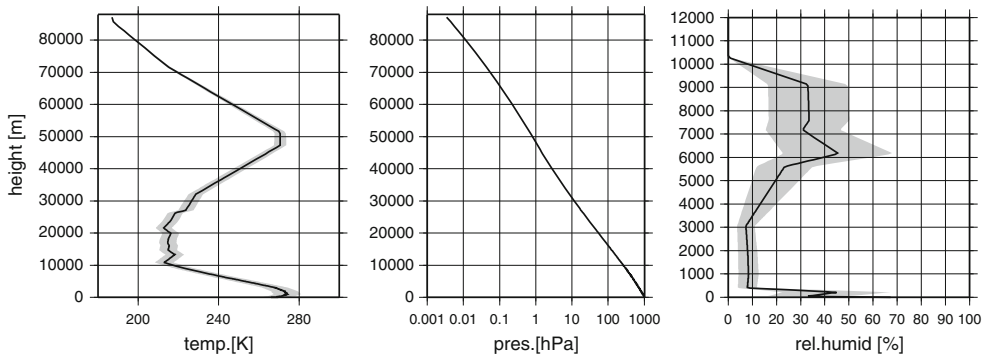

Fig. 2 Temperature (*left*), pressure (*middle*) and relative humidity (*right*) profiles extracted from the meso-scale analysis model (MANAL) from the Japanese Meteorologic Agency (JMA) for a grid point located close to Sapporo, Japan on 1 January 2008, 0 h UT. Pressure and temperature were extrapolated to 86 km height using the US Standard Atmosphere model. The *gray shaded area* shows the range of change when the constituents are varied by ±2.5, ±50 and ±0.25%, respectively, over a spherical distance of 1°. For the temperature profile changes are also scaled with height to take into account that less variations are taking place in higher regions (see text)

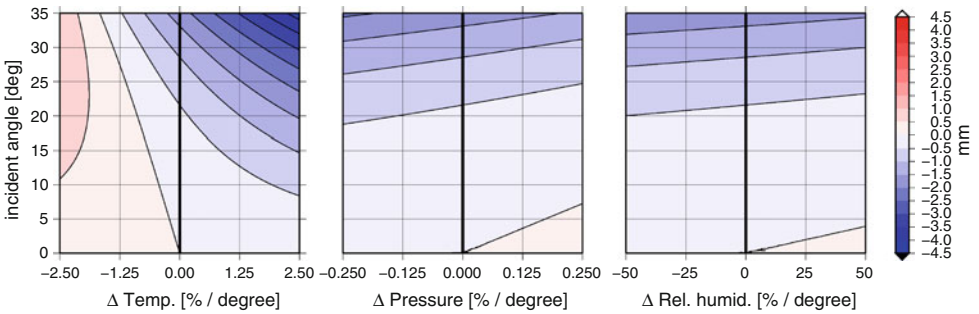

Fig. 3 Difference in integrated atmospheric delay (mm) between the mapping approach and exact ray-tracing when one of the three atmospheric constituents is changing with a horizontal gradient (measured in %/°). *Bold vertical lines* denote the isotropic case

ray-tracing. In the case of lateral temperature variations such an error can become up to four times larger depending on the strength of the horizontal gradient and the incident angle (see Fig. 3, left part). Since pressure variations are expected to be less significant over short distances, we can see that there is hardly any difference between the two approaches (Fig. 3, middle plot). The same holds for the results of relative humidity changes, depicted in the right plot of Fig. 3, where even smaller dependency on the strength of the gradient can be found. Nevertheless, this result is in good agreement with what someone can expect. As the cloud boundary is located below 10 km, even the steepest incident angles lead to a spherical distance of less than 0.1°. Thus, relative humidity changes only by a maximum of 5%, which does not reflect a realistic weather situation with complex wet refractivity fields. Therefore, a second simulation study was carried out, allowing to take sudden humidity changes into account. Thereby, the relative humidity inside a cone with a spherical distance of 0.02° (roughly 2 km) is assumed to be identical to the one in zenith direction as given in Fig. 2. The humidity values outside this cone were modified by ±50%, evoking a jump-like change of wet refractivity as it occurs for the case of rain fronts. Other than the case of long-scale refractivity gradients (results depicted in Fig. 4) it can be seen that large differences between the mapping approach and the exact ray-tracing exist. Except for incident angles close to zenith, where no sudden changes of refractivity occur, the mapping approach works well. For all other situations millimeter order errors are introduced as the off-zenith rays pass regions with more or less wet refractivity. Therefore, the mapping approach will only work well if SAR images are taken with incident angles very close to zenith. Moreover, using small-scale numerical weather models does not improve the situation when using the mapping strategy, as the gain of spatial information is lost by computing troposphere delays not along their true ray-path. Considering the sum of gradient-like effects and the impact of small-scale atmospheric structure errors, up to one centimeter per image are possible. Since InSAR images are always interpreted as the difference between data taken at different epochs, such biases can be damped or magnified depending on the observing geometry and the prevailing atmospheric situation.

3.2 Ray-tracing considerations for fine-mesh models

Since fine-mesh models are usually restricted in their spatial extent it is mandatory to make sure that rays are not leaving the model domain and/or to embed such models in a coarser NWM. Since we are dealing with total troposphere delays, rather than only utilizing the wet delay

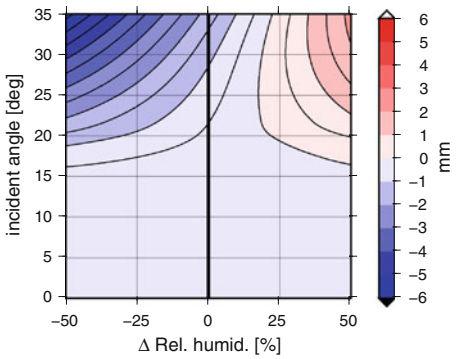

Fig. 4 Same as Fig. 3 (*right plot*). Relative humidity is not modeled by a linear gradient but changes suddenly after a spherical distance of 0.02°

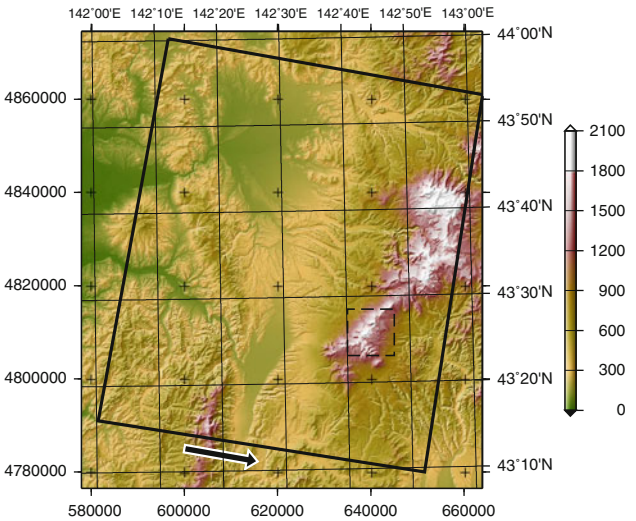

Fig. 5 Topography of the test field, located on Hokkaido, Japan. *Solid black line* shows the area covered by the ALOS/PALSAR images. *Dashed black zone* marks the location around the Tokachi-dake volcano, as shown later in Fig. 9 in detail

contribution, it is important to know the refractivity field above the fine-mesh model. Small-scale refractivity structures will not occur above 10 km of height, but large-scale gradients, mainly caused by pressure variations, can introduce biases in the computed delays. Although these biases are likely to be canceled out when differential corrections for InSAR data are formed, ray-tracing is going to be carried out up to a height of 86 km. Thereby one can apply a nesting approach, as described in Hobiger et al. (2010), which allows to embed the fine-mesh NWM in data from a coarser model. Since incident angles usually do not exceed 40°, the spatial extent of the fine-mesh model should only cover the area of interest, i.e., the region scanned by the SAR satellite, allowing for some buffer zone around the model (see Hobiger et al. 2010).

4 A case study

Mt. Tokachi-dake is an active volcano on Hokkaido island, Japan. While a regional GPS network by JMA has detected inflating signals near the vent (Japan Meteorological Agency 2009), we confirmed the uplifting signals by interferograms in Fig. 9. Since the area has been repeatedly monitored by ALOS/PALSAR (Shimada et al. 2008), the area is a suitable test-bed. As we want to show that the choice of the troposphere correction can impact the interpretation of the underlying geophysical signal we were looking for a region with active ground movement, which we found in studying the Tokachi-dake volcano. Moreover, dedicated model runs of the Cloud Resolving Storm Simulator (CReSS, Tsuboki and Sakakibara 2002) provided 1 km fine-mesh model data as base for the ray-tracing and mapping, respectively. Figure 5 depicts the topography of the concerned area, and displays the zone scanned by the SAR. The images were taken with an average incident angle of 38.79° from an azimuth direction of 100°. The two PALSAR images, from 24 September 2006, 0105 hours UT and 14 August 2008, 0103 hours UT are used to monitor the uplift of the volcano. Since both scans were made during the hot and humid summer, one can expect to have a noticeable impact of varying refractivity inside the InSAR image. Moreover, since the incident angle is very large (even slightly exceeding the range of the simulations carried out in Sect. 3.1), visible differences between the mapping and exact ray-tracing approaches are anticipated.

4.1 Results

For both images, dedicated CReSS model runs with a horizontal resolution of 1 km for the concerned area were provided by the National Research Institute for Earth Science and Disaster Prevention (NIED), Japan. Since these models only reach up to 20 km height, the outer area has been covered by meso-scale analysis model data, which has been interpolated to the concerned epochs. Based on these data-set three different type of corrections for the InSAR image have been computed for each epoch and then differenced to obtain the corrections corresponding to the InSAR image. First, total zenith delays were obtained by vertical integration through the 3D refractivity field, whereas the identical algorithm as used for the ray-tracing later has been applied to avoid inconsistencies. These vertical delays were mapped into the direction of the satellite, using a mean elevation angle valid over the whole area at each epoch (hereafter named "mapped-mean"). In a second run, these vertical delays were mapped with the local (true) elevation angle (named "mapped-true") considering lateral and vertical variation of the pixels on the ground surface with respect to the satellite. Besides these two

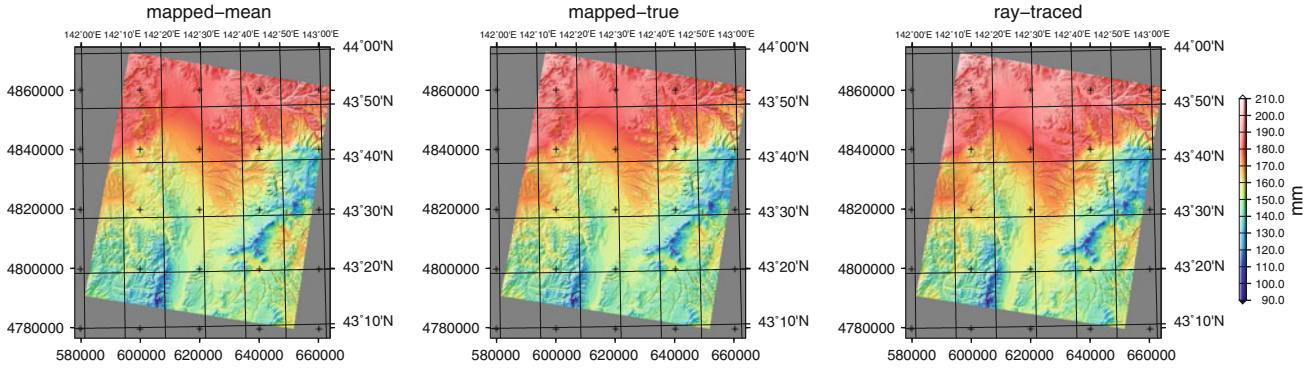

Fig. 6 Troposphere corrections in millimeter for the InSAR image pair (see text). *Left plot* shows the results obtained after mapping the vertically integrated refractivity field with a mean incident angle into the direction of the satellite at each epoch. *Middle plot* shows the corrections when mapping is done with the true incident angle at each ground pixel and the *right figure* depicts the corrections after ray-tracing

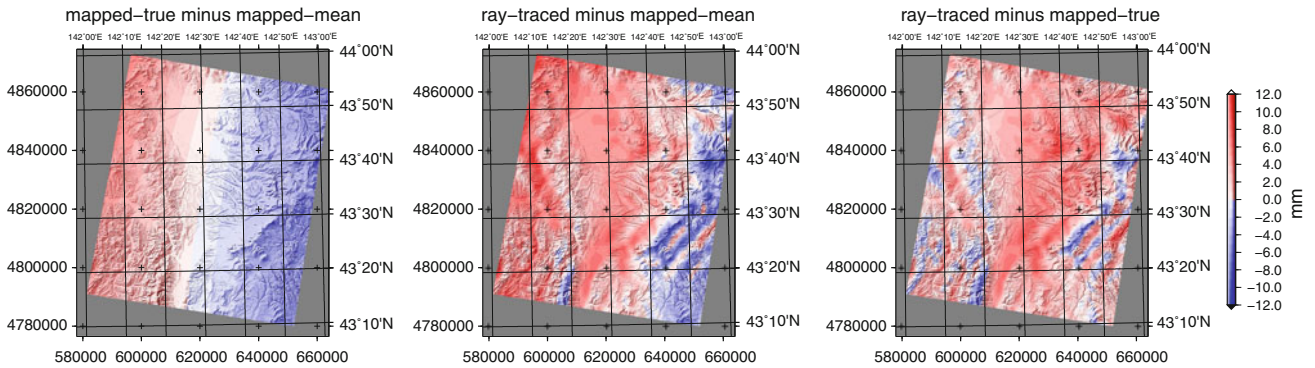

Fig. 7 Differences between the three different computation methods. The left plot shows how the two mapping approaches differ, revealing a linear trend across the image. Differences with respect to the ray-traced corrections (*middle and right plots*) show that centimeter order errors are introduced when any kind of mapping approach is applied instead

mapping approaches, also ray-traced slant delays based on the solution of the Eikonal equation (2) were computed. In the following discussion, all results are based on the difference between the later epoch minus the prior epoch. Figure 6 shows the computed corrections from all three strategies. Although the hydrostatic component of a single image causes the corrections to follow strongly the topography the situation can be more complex for InSAR results as they reflect the differences at two given epoch rather than an absolute measure. To reveal how the three approaches change between each other differences of the obtained corrections are computed and plotted (Fig. 7) for such InSAR data. The differences between the two mapping approaches (left plot in Fig. 7) are as expected caused by the varying elevation angles which related the vertical integrated quantities to slant delays. Since the elevation angle differs for each pixel on the ground with respect to the satellite, mapping with a mean elevation angles introduces a large-scale slope (in first order approximation) instead of the case that delays are mapped with the true incident angles. Since this slope is oriented towards the satellite it could be removed by an additional post-processing step, but changes of incident angles caused by height variation are not absorbed by such a strategy and require more sophisticated handling of the data. Thus, it can be concluded that at least mapping with the exact incident angle, i.e., computing the geometry for each ground pixel, is necessary to avoid large-scale systematic artifacts in the InSAR image.

Comparison of both mapping approaches with the ray-traced corrections shows that small-scale artifacts are likely to be introduced into the images (see center and right plot of Fig. 7). As discussed in the prior section, mapped delays and exactly ray-traced corrections only agree to a certain limit. Caused by lateral gradients of the troposphere, refractivity along the true ray-path differs from that in zenith direction, leading to millimeter order errors of the troposphere corrections. The pattern of these artifacts does not only depend on the observing geometry, but also varies with topographic height of the image pixels. For example, mountain winds

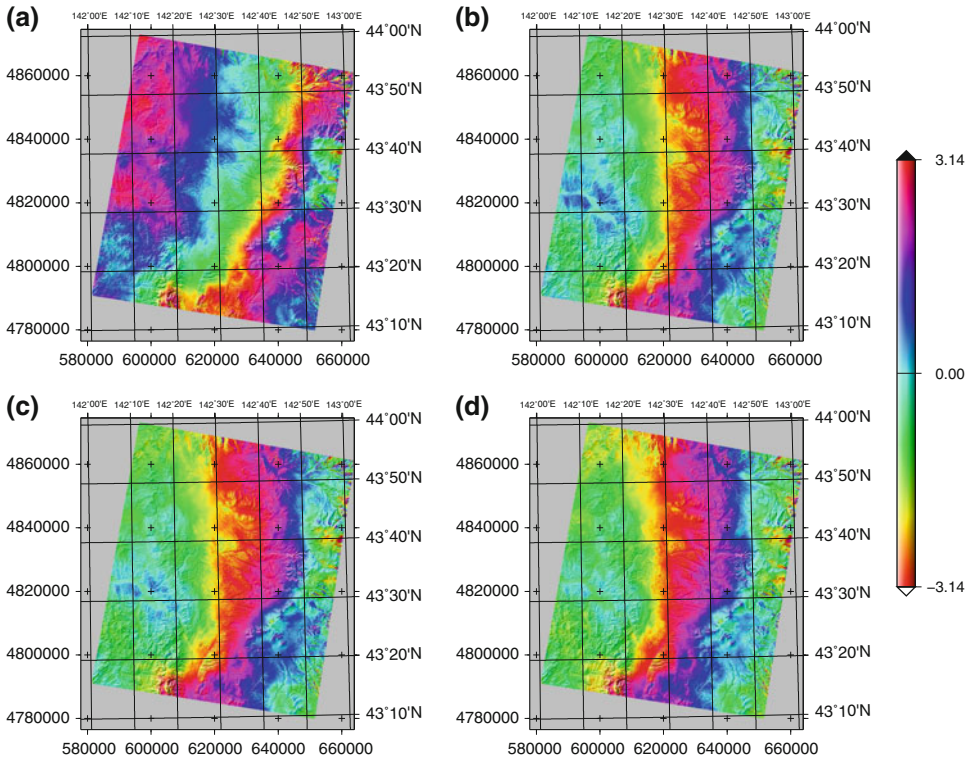

Fig. 8 **a** Unwrapped InSAR image, without any troposphere correction. **b**, **c** Show the results when corrections based on mapping with mean and true incident angles are applied. **d** Depicts the obtained image after introducing the ray-traced correction. All results displayed in units of radians (corresponding wavelength of 23.6 cm, using a cyclic coloring scheme.)

can disturb atmospheric conditions and move air masses up or down depending on the wind direction. Thus, when comparing the mapping approach with direct ray-tracing we face the situation that the atmosphere conditions are somewhat "mirrored" by the topography. As our test region contains several high mountains it happens that the topography implicitly finds its impact in the differences (depending on the local weather conditions and the direction towards the satellite).

Whereas the differences between ray-traced and mapped corrections based on a mean elevation angle are larger than those using exact incident angles for the slant delay conversion, both approaches show the same pattern, but with slightly different amplitudes. Since troposphere InSAR corrections reflect the differences of the atmospheric conditions at two different epochs, and because all three constituents (i.e., pressure, temperature and relative humidity) are showing different lateral gradients, it is not straightforward to assign the differences of the corrections to a clear origin. Basically, the sum of lateral pressure, temperature, and relative humidity variations as discussed in Sect. 3.1, sums up to the total error introduced by the mapping approach. Whereas for some situations the errors cancel out, they are magnified for others. Thus, it is not a surprise that the magnitude of the differences shown in Fig. 7 is nearly three times as large as the one obtained for single troposphere constituent variations in Sect. 3.1.

4.2 Implications for the correction of InSAR images

In order to verify the goodness of each approach, troposphere corrections based on the three different strategies are subtracted from the InSAR image. The InSAR image pair based on data from 24 September 2006, 0105 hours UT and 14 August 2008, 0103 hours UT has been processed with four different strategies. First, no troposphere corrections at all have been applied, thereafter troposphere delays corrections from the three different strategies described before have been used to compensate for atmospheric effects before analyzing the data. Figure 8 shows the unwrapped images for these four strategies. Due to the fact that un-modeled orbit errors remain as long wave-length signals in the images (Hanssen 2001) it can be clearly seen that if no troposphere correction is applied, the range virtual ground motion covers at least two cycles. On the other hand, as soon as any kind of troposphere correction is applied, mainly artifacts caused by orbit modeling errors remain inside the images. Nevertheless, one can see that mapping approach based on an average incident angles tends to underestimate the delays in the Eastern parts, and slightly provides too large corrections in other areas. This is in good agreement with the pattern of the differences found between the mappings based on mean and exact incident angles (left plot in Fig. 7). When comparing the results based on exact mapping with those obtained after correcting with ray-traced delays, these features are reduced further.

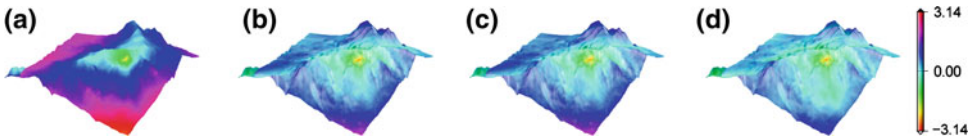

Fig. 9 Three-dimensional perspective view, zooming into the area marked by *dashed lines* in Fig. 5. Ordering of the plots and color scheme are identical to Fig. 8

Since a significant geophysical signal can be expected around the location of the volcano, one can study this area in detail, trying to qualify the four different approaches concerning their usability for the interpretation of the ground motion.

4.2.1 Detection of ground motion

Figure 9 shows the topography around the Tokachi-dake volcano as a 3D perspective view, using the area marked by dashed lines in Fig. 5. Unwrapped phases are draped on the surface using the same color scheme as applied in Fig. 8. Although the image, which has been obtained without any troposphere correction, reveals the uplift on the falling edge of the mountain, the surrounding phases are biased by the missing atmospheric correction, which leads to a misinterpretation of the geophysical signal, revealing a too large ground motion, rather than a quite localized phenomena. The solutions based on any kind of troposphere delay correction help to clearly identify the geophysical signal, whereas the differences between the three approaches are small. The ray-tracing approach differs from the mapping strategies by up to ±1 cm in the concerned area (Fig. 7) which accounts for roughly 0.13 radian in the images. Therefore, the two results based on either mapping strategy look very similar, but the InSAR images obtained after applying ray-traced corrections reveals a slightly different ground movement pattern on the mountain slope.

4.2.2 Reduction of troposphere noise

Other than the visual qualification of the images, it is possible to check the impact of troposphere delay corrections by looking at the data in the spectral domain (Foster et al. 2006). Figure 10 shows the spectra of variances for all four processing strategies, after removing a quadratic trend in order to ensure that orbit errors will not be included in the resulting spectra. Similar to Foster et al. (2006) one can see that the application of the external troposphere delay corrections reduces spectral power. Especially for wavelengths of 4 km or longer troposphere corrections help to reduce the atmospheric signatures. Although the numerical weather model has a spatial resolution of 1 km, improvement down to this wavelength was not expected as the effective resolution is two to three times larger than the nominal one. This is in good agreement with the spectra where we find improvement down to such scales (i.e., 2–3 km). Since the images were de-trended before computing the spectra the slope introduced by the mapping approach based on a mean elevation angle is compensated as well. Thus both mapping approaches lead to nearly identical spectral characteristics of the images. Looking at the ray-tracing approach reveals that additional spectral power at longer wavelengths (between 6 and 60 km) is slightly removed from the images. These results are in good agreement with the spatial extent of the pattern shown in Fig. 7, confirming that exact ray-tracing is preferable to any kind of mapping approach. Other than accessing the noise level in the spectral domain, one can also derive the empirical semi-variogram (Clark 1979)

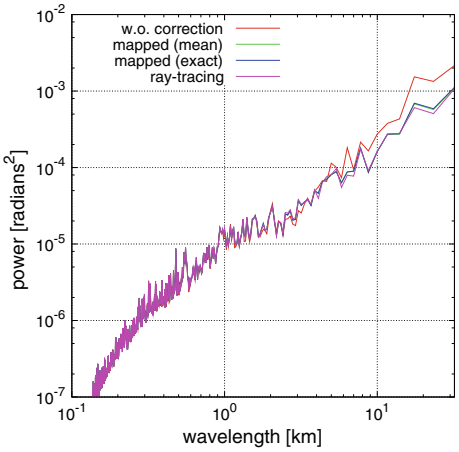

Fig. 10 Spectrum of variances (in cycles) for all four processing strategies after de-trending the images in order to compensate for orbit errors. Thereby a removal of troposphere noise on wavelengths over 6 km is confirmed when numerical weather models are used for the computation of troposphere delays. Ray-traced corrections perform slightly better than the two mapping approaches, which achieve similar results

$$\gamma(h) = \frac{1}{2N(h)} \sum_{1}^{N(h)} (f(x) - f(x+h))^2 \tag{4}$$

which computes the variance of all pixel pairs at a given distance h. Using the de-trended unwrapped phases from all four approaches allows to compute such semi-variograms, as shown in Fig. 11. Thereby, the ray-traced corrections yield again the best performance, i.e., showing less variance than the two other troposphere mitigation approaches.

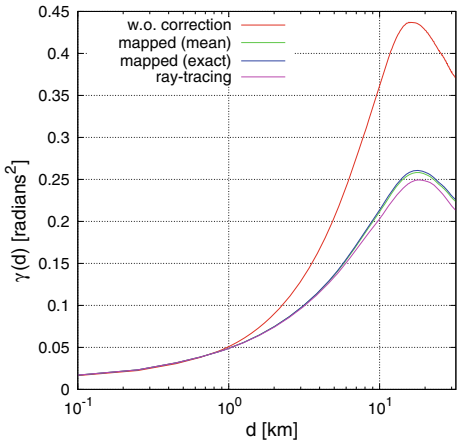

Fig. 11 Semi-variograms (in cycles) for all four processing strategies after de-trending the images. Ray-traced corrections perform better than the two mapping approaches, which achieve nearly similar results

5 Conclusions

Interferometric SAR suffers, like all remote sensing techniques, from the fact that electro-magnetic waves are delayed when passing through the atmosphere. If not compensated, such biases will remain as artifacts in the obtained images and can lead to misinterpretation of the geophysical origin which causes ground motion. In the recent years, numerical weather models have been utilized to correct for troposphere delay errors allowing to remove nearly all of the atmospheric disturbance in the InSAR images. Since ray-tracing for each pixel per image is a time-consuming task many studies relied on the assumption that vertical integration and mapping into slant directions provides information accurate enough for the correction of the images. As atmospheric conditions in zenith and slant direction can vary significantly even over small scales, this approach is limited in its accuracy. Based on arbitrary profiles of atmospheric constituents we are able to show that lateral gradient as well as rapid changes of wet refractivity (i.e., water vapor) leads to errors of the mapping approach which can sum up more than 10 mm. Moreover, it has been demonstrated that, if one relies on the mapping approach at least the true incident angle has to be applied in order to avoid that large-scale biases (i.e., slopes or ring-like structures) are evoked when using only one (mean) incident angle over the whole image. Applying the atmospheric corrections to real InSAR data confirms that ray-traced data are preferable to any kind of mapping approach, leading to less noise in the cleaned images. Since numerical weather models are continuously improving concerning their spatial resolution, it becomes more and more important to replace any mapping approach with exact ray-tracing in order to take full advantage of the model. Other than the complex ray-tracing solution discussed here, one might also compute corrections via integrating along the line-of-sight between the ground point and the satellite. This approach would be faster and yield similar results as the ray-tracing approach, but can only be applied when bending angle effects can be neglected. Such a neglecting is valid if the local incident angles are small enough, which is true for most of the current remote sensing applications. On the other side, integration along the line-of-sight will only be valid if gradients along this path are small enough not to introduce errors. Moreover, out-of-plane bending effects and the valuable information contained in fine-mesh models might not be properly considered by such a simplification which suggests that the exact solution of the ray-path is more straightforward concerning future applications.

6 Outlook

One of the main concerns of ray-tracing for InSAR and a factor why it is not applied in standard processing is that computations are very time-consuming. As suggested by Hobiger et al. (2009) the usage of low-cost off-the-shelf graphic cards might be one solution which helps to reduce computation time drastically and make this approach more attractive on standard PC platforms. Besides the computational aspects, atmospheric corrections can only be as good as the numerical weather model is able to give an accurate representation of the refractivity field. Since weather models are strongly depending on the selection of the initial conditions, the quality and validity of the model physics, one has to select a proper model carefully and if possible run a model which is best suitable for the concerned area. Moreover, assimilation of external data becomes more and more important in the future and the incorporation of troposphere information from ground- and space-based GPS receivers is expected to improve the accuracy of numerical weather models further towards a very close representation of the real-world atmospheric conditions.

Acknowledgments The authors would like to thank the Editor-in-Chief and the anonymous reviewers for their valuable comments which helped to improve this paper. The ownership of PALSAR data belongs to the Ministry of Economy, Trade and Industry and JAXA. PALSAR level 1.0 data used in this study were provided from the PALSAR Interferometry Consortium to Study our Evolving Land surface (PIXEL) under a cooperative research contract of Earthquake Research Institute, University of Tokyo with JAXA. Parts of this work were supported by a Grant-in-Aid for Scientific Research (KAKENHI-21241043) as well as YK and MF are supported from KAKENHI (19340123). The authors are grateful to the National Research Institute for Earth Science and Disaster Prevention for providing us with numerical weather model data. Figures were made with the Generic Mapping Tools of Wessel and Smith (1991), Inkscape (http://www.inkscape.org) and GNUPLOT (http://www.gnuplot.info).

References

Boudouris G (1963) On the index of refraction of air, the absorption and dispersion of centimeter waves by gases. J Res Natl Bur Stand 67:631–684

Clark I (1979) Practical geostatistics. Applied Science Publishers Ltd, London

Foster J, Brooks B, Cherubini T, Shacat C, Businger S, Werner CL (2006) Mitigating atmospheric noise for InSAR using a high resolution weather model, Geophys. Res Lett 33:L16304. doi:10.1029/2006GL026781

Fujiwara S, Tobita M, Murakami M, Nakagawa H, Rosen PA (1999) Baseline determination and correction of atmospheric delay induced by topography of SAR interferometry for precise surface change detection (in Japanese with abstract and figures in English). J Geod Soc Jpn 45(4):315–325

Furuya M, Mueller K, Wahr J (2007) Active salt tectonics in the Needles District, Canyonlands (Utah) as detected by interferometric synthetic aperture radar and point target analysis: 1992–2002. J Geophys Res 112:B06418. doi:10.1029/2006JB004302

Hanssen R (2001) Radar interferometry: data interpretation and error analysis. Kluwer, The Netherlands

Hobiger T, Ichikawa R, Koyama Y, Kondo T (2008) Fast and accurate ray-tracing algorithms for real-time space geodetic applications using numerical weather models. J Geophys Res 113:D20302. doi:10.1029/2008JD010503

Hobiger T, Ichikawa R, Koyama Y, Kondo T (2009) Computation of troposphere slant delays on a GPU. IEEE Trans Geosci Remote Sens 47(10):3313–3318. doi:10.1109/TGRS.2009.2022168

Hobiger T, Shimada S, Shimizu S, Ichikawa R, Koyama Y, Kondo T (2010) Improving GPS positioning estimates during extreme weather situations by the help of fine-mesh numerical weather models. J Atmos Solar Terr Phys 72(2–3):262–270. doi:10.1016/j.jastp.2009.11.018

Japan Meteorological Agency (2009) Monthly Volcanic Activity Report (in Japanese). http://www.seisvol.kishou.go.jp/tokyo/STOCK/monthly_v-act_doc/monthly_vact.htm

Paris DT, Hurd FK (1969) Basic electromagnetic theory. McGraw-Hill, New York

Shimada M, Ozawa T, Fukushima Y, Furuya M, Rosenqvist A (2008) Japanese L-band radar improves surface deformation monitoring. EOS Trans AGU 89:277–278

Smith EK, Weintraub S (1953) The constants in the equation for atmospheric refractive index at radio frequencies. J Res Natl Bur Stand 50:39–41

Tsuboki K, Sakakibara A (2002) Large-scale parallel computing of cloud resolving storm simulator. High Perform Comput 243–259. doi:10.1007/3-540-47847-7_21

Wadge G, Webley PW, Bingley R, Dodson AH, James IN, Waugh S, Veneboer T, Puglisi G, Mattia M, Baker D, Edwards SC, Edwards SE, Clarke P (2002) Atmospheric models, GPS, and InSAR measurements of the tropospheric water vapour field over Mount Etna. Geophys Res Lett 29(19):1905. doi:10.1029/2002GL015159

Wessel P, Smith WH (1991) Free software helps map and display data. EOS Trans AGU 72:441

World Meteorological Organization (2000) General meteorological standards and recommended practices. Appendix A, WMO Technical Regulations, WMO-No. 49, corrigendum, August 2000